

# COUPLED HYDRO-THERMAL-MECHANICAL ANALYSIS FOR COLD CO<sub>2</sub> INJECTION INTO A DEEP SALINE AQUIFER

by

*Huimin WANG<sup>a,c</sup>, J.G. WANG<sup>a,b\*</sup>, Xiaolin WANG<sup>c</sup>, Fakai DOU<sup>a</sup>, and Bowen HU<sup>b</sup>*

<sup>a</sup>State Key Laboratory for Geomechanics and Deep Underground Engineering, China University of Mining and Technology, Xuzhou 221116, China

<sup>b</sup>School of Mechanics and Civil Engineering, China University of Mining and Technology, Xuzhou 221116, China

<sup>c</sup>School of Engineering, University of Tasmania, Hobart, Tasmania 7001, Australia

*This study investigated the thermal effects of thermal stress and Joule-Thomson cooling on CO<sub>2</sub> migration in a deep saline aquifer through a hydro-thermal-mechanical model. Firstly, the temperature variation of injected CO<sub>2</sub> was analyzed through the coupling of two-phase flow, deformation of porous medium and heat transfer with Joule-Thomson effect. Then, the effect of capillary entry pressure on CO<sub>2</sub> plume was numerically investigated and compared. It is found that injection temperature and Joule-Thomson effect can significantly affect the distributions of CO<sub>2</sub> mass and temperature, particularly in the upper zone near the injection well. The reduction of capillary entry pressure accelerates the upward migration of CO<sub>2</sub> plume and increases the CO<sub>2</sub> lateral migration distance.*

Key words: CO<sub>2</sub> storage, two-phase flow, Joule-Thomson effect, thermal stress, multi-physical process

## Introduction

Carbon Capture and Storage (CCS) has become one of the most effective choices to reduce greenhouse gas emissions [1, 2]. Deep geological aquifers were widely used as CO<sub>2</sub> storage reservoirs [3]. The long-term sequestration of CO<sub>2</sub> in the reservoir is safeguarded by the sealing efficiency of overlying caprocks. The behavior of CO<sub>2</sub> flow in the storage reservoir is the first step to the success of CO<sub>2</sub> sequestration [4]. Current analysis for the first step usually assumes a constant temperature of reservoir (called isothermal process later). In this isothermal process, the physical properties (density and viscosity) of CO<sub>2</sub> do not change with temperature. However, heat transfer is a complex process with strong nonlinearity [5, 6]. Such an assumption of isothermal process may affect the prediction accuracy of CO<sub>2</sub> flow behavior.

Injected CO<sub>2</sub> is usually colder than the reservoir. This causes thermal contraction and

---

\* Corresponding author, email: jgwang@cumt.edu.cn; nuswjg@yahoo.com

thermal stress [7, 8]. When high-pressure CO<sub>2</sub> is injected into the low-pressure reservoir, the CO<sub>2</sub> expands, causing further temperature drop due to Joule-Thomson cooling. Vilarrasa et al. [9] compared the flow behaviors of liquid CO<sub>2</sub> and supercritical CO<sub>2</sub> in the reservoir. They found that the injection efficiency of liquid CO<sub>2</sub> is higher due to higher density of liquid CO<sub>2</sub> and smaller resultant overpressure. This indicates that the change of CO<sub>2</sub> physical properties during injection is indeed worth of multi-physical modeling. Mathias et al. [10] developed a simple analytical solution and found that Joule-Thomson cooling is a negative factor for CO<sub>2</sub> storage. In this solution, the permeability of reservoir is constant and the accumulation of pore pressure and the thermal stress were not considered. Gao et al. [11] proposed traveling-wave solutions for both linear and non-linear heat transfers. They only considered the temperature variation without the thermal-mechanical coupling. This is not enough to understand the CO<sub>2</sub> flow behaviors in the geological storage. Gor et al. [12] established a multi-phase model to investigate the effect of thermal stress on caprock integrity. Their simulations showed that the stress above the horizontal injection well may lead to tensile or shear failure of the caprock. Kim and Hosseini [7] conducted a numerical simulation to include fluid flow, thermal stress and thermal diffusion. However, their simulation was based on single-phase flow. The effects of relative permeability parameters on CO<sub>2</sub> migration in the reservoir have not been included. The above studies have demonstrated the importance of non-isothermal flow of CO<sub>2</sub> in a deep saline aquifer, but a coupled hydro-thermal-mechanical model is still missing.

This study will extend our previous two-phase flow model [18] to include the thermal stress and Joule-Thomson effects. Thermal stress is included in a new porosity model to investigate the matrix shrinkage caused by cold CO<sub>2</sub> injection. The Joule-Thomson effect is considered in the changes of CO<sub>2</sub> physical properties. Further, the effect of capillary entry pressure on CO<sub>2</sub> migration is also included in the model.

## Governing equations for non-isothermal two-phase flow

### *Mass conservation equation for two-phase flow*

The mass conservation laws for the flow of water and CO<sub>2</sub> in porous medium are [13, 14]

$$\frac{\partial(\phi\rho_w s_w)}{\partial t} + \nabla \left[ -\frac{kk_{rw}}{\mu_w} \rho_w (\nabla p_w + \rho_w g \nabla H) \right] = Q_w, \quad (1)$$

$$\frac{\partial m}{\partial t} + \nabla \left[ -\frac{kk_{rg}}{\mu_g} \rho_g (\nabla p_g + \rho_g g \nabla H) \right] = Q_g, \quad (2)$$

and

$$m = \phi \rho_g s_g + \rho_{ga} \rho_c \frac{V_L p_g}{p_L + p_g} \exp\left(-\frac{c_1 \Delta T}{1 + c_2 p_g}\right), \quad (3)$$

where  $\phi$  is the porosity,  $s_w$  is the saturation of water,  $p_w$  is the water pressure,  $p_g$  is the gas pressure,  $\rho_w$  is the density of water,  $\rho_g$  is the density of CO<sub>2</sub>,  $k$  is the intrinsic permeability,  $k_{rw}$  is the relative permeability of water,  $k_{rg}$  is the relative permeability of gas,  $\mu_w$  is the viscosity of water,

$\mu_g$  is the viscosity of gas,  $g$  is the gravitational acceleration,  $H$  is the elevation in vertical direction,  $Q_w$  is the source of water,  $Q_g$  is the source of CO<sub>2</sub>,  $s_g$  is the saturation of CO<sub>2</sub>,  $\rho_c$  is the density of rock,  $\rho_{ga}$  is the CO<sub>2</sub> density under the standard conditions,  $V_L$  is the Langmuir volume constant,  $p_L$  is the Langmuir pressure,  $c_1$  is the temperature correction coefficient of gas adsorption (K<sup>-1</sup>), and  $c_2$  is the pressure correction coefficient of gas adsorption (MPa<sup>-1</sup>).

The density of CO<sub>2</sub> is

$$\rho_g = \frac{M_{CO_2}}{ZRT} p_g, \quad (4)$$

where  $M_{CO_2}$  is the molecular weight of CO<sub>2</sub>,  $R$  is the universal gas constant,  $T$  is the gas temperature, and  $Z$  is the compressibility factor of real gas.

Since the pressure and the temperature of CO<sub>2</sub> in this study vary in a certain range (14MPa-26MPa;310K-324K). The compressibility factor  $Z$  can be defined as an interpolation factor for the computation in Comsol Multiphysics. The compressibility with respect to temperature and pressure can be derived as

$$c_T = \frac{1}{\rho_g} \frac{\partial \rho_g}{\partial T} = - \left( \frac{1}{T} + \frac{1}{Z} \frac{\partial Z}{\partial T} \right), \quad (5)$$

and

$$c_p = \frac{1}{\rho_g} \frac{\partial \rho_g}{\partial p_g} = \left( \frac{1}{p_g} - \frac{1}{Z} \frac{\partial Z}{\partial p_g} \right). \quad (6)$$

Heidaryan et al.[15] developed a formula to calculate the CO<sub>2</sub> viscosity in ranges of pressure (7.5-101.4 MPa) and temperature(310-900 K):

$$\mu_g = \frac{A_1 + A_2 + A_3 p_g^2 + A_4 \ln(T) + A_5 (\ln(T))^2 + A_6 (\ln(T))^3}{1 + A_7 p_g + A_8 \ln(T) + A_9 (\ln(T))^2}, \quad (7)$$

where the pressure and the temperature are expressed in bar and K, respectively. The viscosity unit is centipoise (cp). Unit conversion is required before calculation.  $A_1 - A_9$  are the tuned coefficients [15]. Substituting eqs. (3), (4), (5), (6) into eqs. (1) and (2) obtains the final governing equations of two-phase flow as follows

$$\phi c_s \frac{\partial p_g}{\partial t} - \phi c_s \frac{\partial p_w}{\partial t} + \nabla \left[ -\frac{kk_{rw}}{\mu_w} (\nabla p_w + \rho_w g \nabla H) \right] = Q'_w - s_w \frac{\partial \phi}{\partial t}, \quad (8)$$

$$\begin{aligned} & \left[ -\phi c_s + \phi s_g c_p + \frac{\rho_{ga} \rho_c}{\rho_g} \exp \left( -\frac{c_1 \Delta T}{1 + c_2 p_g} \right) \left( \frac{V_L P_L}{(P_L + p_g)^2} - \frac{V_L p_g}{P_L + p_g} \frac{c_1 c_2 \Delta T}{(1 + c_2 p_g)^2} \right) \right] \frac{\partial p_g}{\partial t} + \phi c_s \frac{\partial p_w}{\partial t} \\ & + \nabla \left[ -\frac{kk_{rg}}{\mu_g} (\nabla p_g + \rho_g g \nabla H) \right] = - \left[ \phi s_g c_T \frac{\rho_{ga} \rho_c}{\rho_g} \frac{V_L p_g}{P_L + p_g} \exp \left( -\frac{c_1 \Delta T}{1 + c_2 p_g} \right) \frac{-c_1}{1 + c_2 p_g} \right] \frac{\partial T}{\partial t} - s_g \frac{\partial \phi}{\partial t} + Q'_g \end{aligned} \quad (9)$$

where  $c_s$  is the compressibility with respect to capillary pressure, which is obtained from the relationship of water saturation and capillary pressure. The detail of  $c_s$  can refer to our previous work

[13,14].  $Q_w = \rho_w Q'_w$  and  $Q_g = \beta Q'_g$ ,  $\beta$  is a constant.

### Thermoelastic strain in porous media

The porosity model considering both thermal strain and sorption strain is proposed as

$$\phi = \phi_0 + \alpha \left( \varepsilon_v + \frac{p}{K_s} - \varepsilon_{s1} - \varepsilon_{s2} \right), \quad (10)$$

where  $\phi_0$  is the initial porosity,  $\phi$  is the current porosity,  $\alpha$  is the Biot coefficient,  $K_s$  is the bulk modulus of rock grain,  $p$  is the gas pressure in pores,  $\varepsilon_v$  is the volumetric strain,  $\varepsilon_{s1}$  is the sorption strain, and  $\varepsilon_{s2}$  is the thermal strain.

The evolution of porosity in the two-phase flow is further expressed as

$$\frac{\partial \phi}{\partial t} = \alpha \left( \frac{\partial \varepsilon_v}{\partial t} + \frac{1}{K_s} \frac{\partial p}{\partial t} - \frac{\partial \varepsilon_{s1}}{\partial t} - \alpha_T \frac{\partial T}{\partial t} \right). \quad (11)$$

### Energy conservation for heat transfer

During the injection of CO<sub>2</sub> into the geological reservoir, the heat transfer satisfies the energy conservation [16, 17]

$$\frac{\partial (C_{eq} T)}{\partial t} - \phi \left( \rho_g C_g \mu_{JT} + 1 \right) \frac{\partial p_g}{\partial t} + K \alpha_T T \frac{\partial \varepsilon_v}{\partial t} + \nabla \cdot v_T = 0, \quad (12)$$

where  $K$  is the bulk modulus of porous media,  $\alpha_T$  is the thermal expansion coefficient, and  $\mu_{JT}$  is the Joule-Thomson coefficient.  $C_{eq} = \phi \rho_g C_g + (1 - \phi) \rho_c C_s$  is the specific heat capacity of porous medium.  $v_T$  represents the average heat transfer rate and can be divided into heat conduction and heat convection

$$v_T = -K_{eq} \nabla T + \rho_g C_g \frac{k k_{rg}}{\mu_g} \nabla p_g \left( T - \mu_{JT} p_g \right), \quad (13)$$

where  $K_{eq}$  is the thermal conductivity,  $C_g$  is the specific heat capacity of CO<sub>2</sub>,  $C_s$  is the specific heat capacity of rock.

Substituting eq.(13) into eq.(12) gets the final governing equation of heat transfer as

$$\begin{aligned} & \left( \phi \rho_g C_g + (1 - \phi) \rho_c C_s \right) \frac{\partial T}{\partial t} - \phi \left( \rho_g C_g \mu_{JT} + 1 \right) \frac{\partial p_g}{\partial t} + K \alpha_T T \frac{\partial \varepsilon_v}{\partial t} \\ & = K_{eq} \nabla^2 T + \rho_g C_g \frac{k k_{rg}}{\mu_g} \nabla p_g \left( \nabla T - \mu_{JT} \nabla p_g \right) \end{aligned} \quad (14)$$

### Setup of numerical model

The same geological formation was used by Vilarrasa et al. [9]. We have studied the penetration of CO<sub>2</sub> into the caprock in our previous study [13], thus this study only focuses on the non-isothermal flow of CO<sub>2</sub> in the storage reservoir. As shown in fig. 1, the computational model is composed of a two-dimensional domain and is located at the depth of 1500 m. The domain is 1000 m

long and 100 m high. Its top and bottom boundaries are no-flow. The hydrostatic pressure is initially distributed in the computational domain as initial reservoir pressure. The reservoir temperature is 322.5 K. The cold CO<sub>2</sub> (310 K, still in supercritical state) is injected from the left boundary with a prescribed CO<sub>2</sub> mass flow rate (1.0 Mt/yr). The model parameters are listed in tab.1.

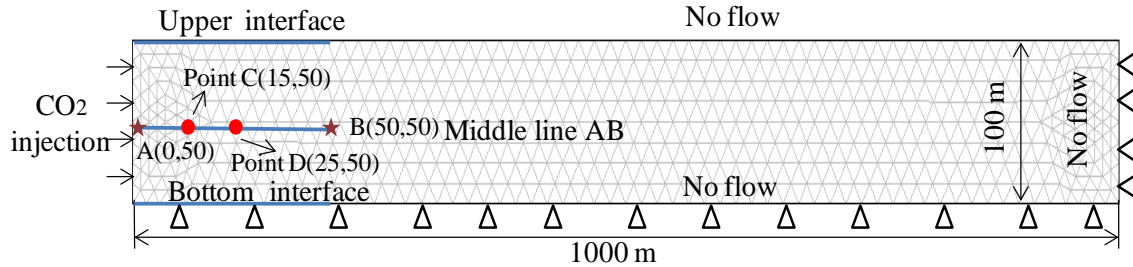


**Figure 1. A two-dimensional computational model**

**Table 1. Model parameters used in computation**

Parameter	Unit	Value	Physical Meanings
$\mu_w$	Pa*s	$5.5 \times 10^{-4}$	Water viscosity
$p_{w0}$	MPa	$10.1 + 0.0102 \times (500 - y)$	Initial water pressure in reservoir
$p_{g0}$	MPa	$p_{w0} + p_e$	Initial CO <sub>2</sub> pressure in reservoir
$p_e$	MPa	0.1	Capillary entry pressure
$T_0$	K	323	Temperature
$k_0$	m <sup>2</sup>	$1 \times 10^{-13}$	Initial absolute permeability
$\phi_0$		0.15	Initial porosity
$\nu$		0.25	Poisson's ratio of shale
$\rho_c$	kg/m <sup>3</sup>	1250	Shale density
$P_L$	MPa	6	Langmuir pressure
$V_L$	m <sup>3</sup> /kg	0.03	Langmuir sorption capacity
$\varepsilon_L$		0.015	Langmuir swelling strain
$\rho_w$	kg/m <sup>3</sup>	1020	Water density
$C_g$	J/(kg*K)	800	Specific heat of CO <sub>2</sub>
$C_s$	J/(kg*K)	900	Specific heat of rock
$\alpha_T$	1/K	$1 \times 10^{-5}$	Coefficient of thermal expansion
$\mu_{JT}$	K/MPa	0.7	Joule-Thomson coefficient

## Results and Discussions

### *Temperature evolution near the injection well*

When a large amount of cold CO<sub>2</sub> is injected into the reservoir, the profile of temperature will change with heat transfer, especially near the injection well. Fig. 2 is the temperature distribution along the AB line after 1 month, 6 months and 1 year of CO<sub>2</sub> injection. After 1 month of CO<sub>2</sub> injection, the temperature influence range is less than 10m. After one year, the range is expanded to 50m away

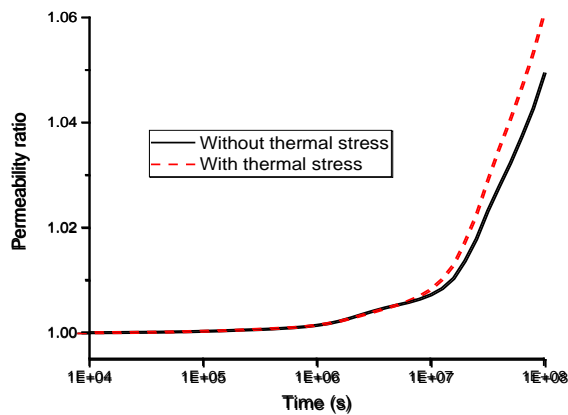
from the injection well. These results indicate that the cold CO<sub>2</sub> injection only affects the temperature in the zone near the injection well. The CO<sub>2</sub> will be in equilibrium with reservoir temperature in a short range of injection well.

Since CO<sub>2</sub> migrates upward under buoyancy, the temperature transfer also shows the coincidence with gas flow. The upper, middle and bottom lines are displayed in the computational model. Fig. 3 shows the distribution of temperature along these three lines after one year of CO<sub>2</sub> injection. Temperature changes are almost the same along the middle and bottom boundaries. However, the temperature distribution at the upper boundary is significantly lower than other two lines. This also indicates that the upward migration of CO<sub>2</sub> causes the temperature decrease in the upper area of the reservoir.

**Figure 2. Distribution of CO<sub>2</sub> temperature near the well**

**Figure 3. Temperature distribution along three horizontal lines at one-year CO<sub>2</sub> injection**

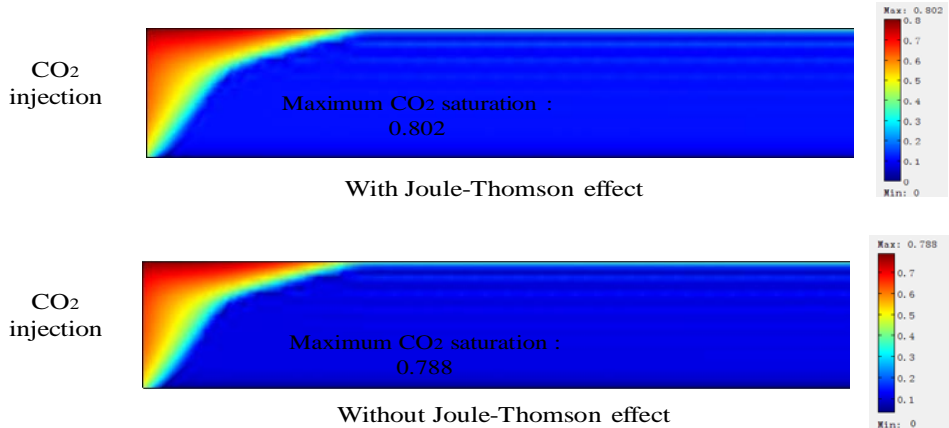
Thermal stress causes the change of permeability in this hydro-thermal-mechanical coupled model. The flow of cold CO<sub>2</sub> brings a cooling effect to the reservoir, so the matrix shrinks and the permeability increases.



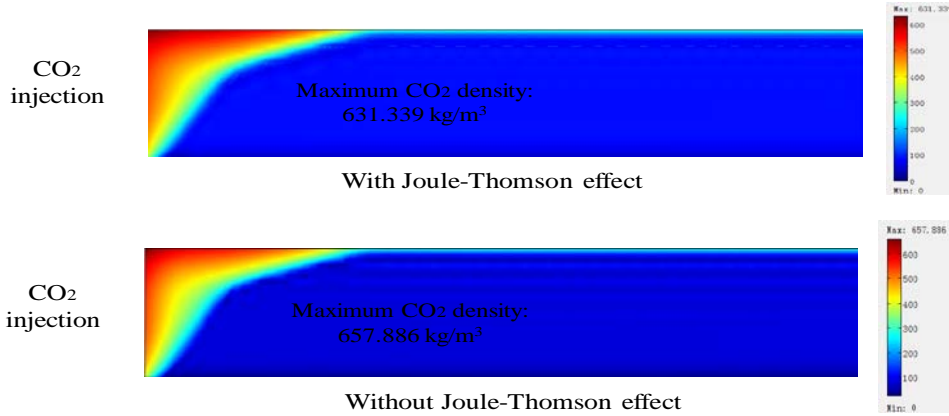
**Figure 4. Comparison of permeability ratio at point C(15,50) with /without thermal stress**

Fig. 4 shows the comparison of permeability ratio at a typical point C (15,50) with and without thermal stress. Since the injection of CO<sub>2</sub> causes an increase in pore pressure, more pore space is opened. The permeability increases whether the flow is isothermal or non-isothermal. However, the permeability increases more at the non-isothermal flow due to thermal stress. This increase of permeability makes CO<sub>2</sub> migrate more easily.

A great pressure drop would occur near the well when CO<sub>2</sub> is injected into the reservoir. Due to the Joule-Thomson effect, this pressure drop can also give rise to a temperature drop. The physical properties of CO<sub>2</sub> (density and viscosity) experience a significant change near the injection well due to the combination action of temperature and pressure drops. The density directly affects the storage efficiency of CO<sub>2</sub> in the reservoir. The viscosity is related to the CO<sub>2</sub> migration in the reservoir and the pressure buildup at the bottom of the caprock. Fig. 5 shows the distributions of CO<sub>2</sub> saturation with or without Joule-Thomson effect after one-year injection. Because the constitutive relationship between saturation and capillary pressure is the same, the front of CO<sub>2</sub> displacing water is almost identical. However, with considering the Joule-Thomson effect, the injected high-pressure CO<sub>2</sub> expands freely and the density decreases. More CO<sub>2</sub> migrates upward under the action of buoyancy. Thus, this CO<sub>2</sub> saturation is higher.



**Figure 5. Distributions of CO<sub>2</sub> saturation after one-year injection**



**Figure 6. Comparisons of the CO<sub>2</sub> effective density after one-year injection**

In order to evaluate this injection efficiency, we define the effective density of CO<sub>2</sub> ( $\rho_e = s_g \rho_g$ ). Fig. 6 gives the comparison of effective density. The CO<sub>2</sub> saturation is higher after considering the Joule-Thomson effect in fig. 5, but the effective density is lower. This implies that Joule-Thomson effect reduces the injection efficiency of CO<sub>2</sub>.

The viscosity of CO<sub>2</sub> is an important parameter related to flow mobility. The viscosity

increases with the accumulation of pressure when high-pressure CO<sub>2</sub> is injected into the reservoir. When the CO<sub>2</sub> injection pressure remains the same, the variations of injection temperature become more important to the CO<sub>2</sub> viscosity. Fig.7 shows the evolutions of CO<sub>2</sub> viscosity with injection temperature of 310, 314 and 318 K. The injected CO<sub>2</sub> is colder, the viscosity is higher. This increase of viscosity makes CO<sub>2</sub> migrate slower in the reservoir.

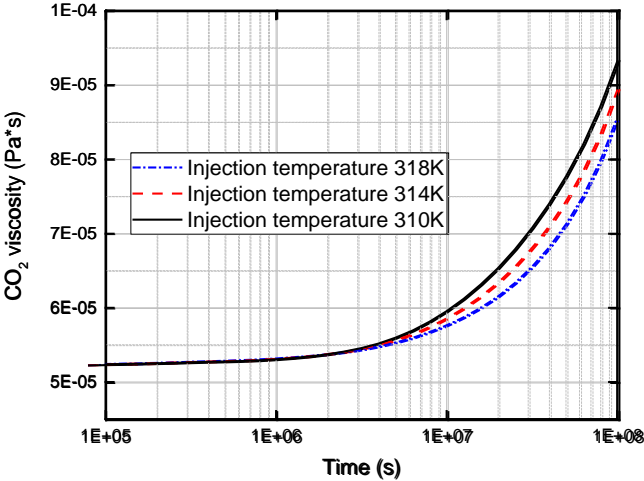


**Figure7. Variation of CO<sub>2</sub> viscosity atpoint D (25, 50) under different injection temperatures**

*Effect of capillary entry pressure on CO2 plume*

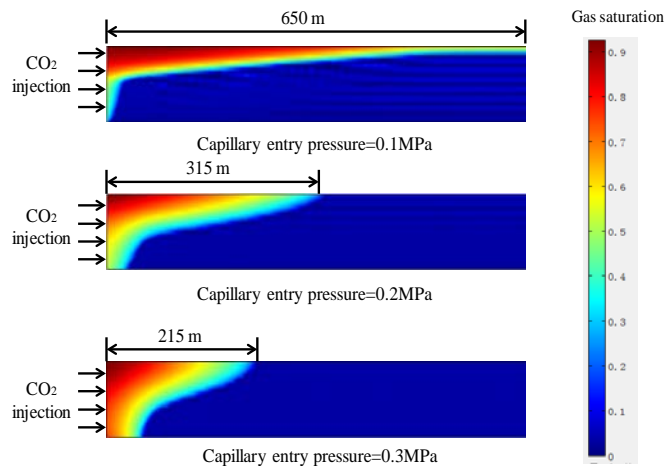
Capillary entry pressure does not only determine the efficiency of CO<sub>2</sub> capillary capture, but also affects the degree of CO<sub>2</sub> displacing water in the caprock. The capillary entry pressure has a wide variation from 0.1 MPa to 48.3 MPa. This value depends on different geological reservoir or caprock. In this study, the capillary entry pressure is assumed to be 0.1, 0.2 and 0.3 MPa, respectively.

Fig. 8 shows the spatial distribution of CO<sub>2</sub> plume after 3 years of CO<sub>2</sub> injection. When the capillary entry pressure is 0.1 MPa, the injected CO<sub>2</sub> firstly migrates upward under the action of buoyancy, and quickly accumulates at the bottom of the caprock and migrates laterally. As the capillary pressure increases, the lateral migration distance of the CO<sub>2</sub> plume is significantly reduced. This implies that capillary entry pressure prevents the spatial migration of CO<sub>2</sub>. In addition, the increase of capillary entry pressure causes the increase of CO<sub>2</sub> capillary storage efficiency. It is found that more CO<sub>2</sub> is sealed in the zone near the injection well instead of migrating upwards.

The migration distance of CO<sub>2</sub> in the lateral direction is related to the accumulation of gas pressure under the caprock. This is important to the CO<sub>2</sub> storage efficiency in the reservoir and will further affect the stability of the caprock in a longer time. Thus, we calculate the lateral migration distance of CO<sub>2</sub> after 3-year injection when the capillary entry pressure is 0.1, 0.15, 0.2, 0.25, and 0.3 MPa, respectively. The results are presented in fig. 9. With the increase of capillary entry pressure, the lateral migration distance of CO<sub>2</sub> decreases significantly. Especially when the capillary entry pressure is below 0.2 MPa, the lateral migration distance changes dramatically. As the capillary entry pressure



increases, a linear relationship with the lateral migration distance is approximately observed. This indicates that capillary entry pressure is an important parameter to the CO<sub>2</sub> storage efficiency.



**Figure 8. Effect of capillary entry pressure on Figure 9. CO<sub>2</sub> migration distance varies the shape of CO<sub>2</sub> plume after 3-year injection with capillary entry pressure**

## Conclusions

This study extends our previous two-phase flow model to include the thermal effects (thermal stress and Joule-Thomson cooling). The following conclusions can be drawn: The temperature effect of cold CO<sub>2</sub> mainly occurs near the injection well, and the temperature of the upper interface is lower due to the CO<sub>2</sub> upward migration. The permeability ratio of non-isothermal flow is 1.1% higher than that of isothermal flow due to thermal stress; The density of CO<sub>2</sub> decreases slightly with considering the Joule-Thomson effect. The injected CO<sub>2</sub> temperature is lower, and the viscosity is greater; Capillary entry pressure affects the shape of CO<sub>2</sub> plume. When capillary entry pressure is lower, more CO<sub>2</sub> migrates upward under buoyancy and the CO<sub>2</sub> lateral migration distance is greater.

## Acknowledgments

The authors are grateful to the financial support from the National Natural Science Foundation of China (Grant No. 51674246) and the State Key Research Development Program of China (2016YFC0600705).

## References

- [1] Johnsson, F., *et al.*, The Importance of CO<sub>2</sub> Capture and Storage: a Geopolitical Discussion, *Thermal Science*, 16(2012), 3, pp. 655-668
- [2] Li, C., *et al.*, Coupled Multiphase Thermo-Hydro-Mechanical Analysis of Supercritical CO<sub>2</sub> Injection: Benchmark for the in Salah Surface Uplift Problem. *International Journal of*

- Greenhouse Gas Control*, 51(2016), pp. 394-408
- [3] Wei, X., *et al.*, Modeling the Hydromechanical Responses of Sandwich Structure Faults During Underground Fluid Injection. *Environmental Earth Sciences*, 75(2016), 16, pp.1155-1170
- [4] Mijic, A., *et al.*, CO<sub>2</sub>Injectivity in Saline Aquifers: the Impact of non-Darcy Flow, Phase Miscibility, and Gas Compressibility. *Water Resources Research*, 50(2014), 5, pp. 4163-4185
- [5] Yang, X. J., *et al.*, Some New Applications for Heat and Fluid Flows via Fractional Derivatives without Singular Kernel. *Thermal Science*, 20(2016), Suppl. 3, pp. S833-S839
- [6] Yang, X. J., *et al.*, A New Technology for Solving Diffusion and Heat Equations. *Thermal Science*, 21 (2017), 1A, pp. 133-140
- [7] Kim, S., *et al.*, Hydro-Thermo-Mechanical Analysis During Injection of Cold Fluid into a Geologic Formation. *International Journal of Rock Mechanics & Mining Sciences*, 77(2015), 4, pp. 220-236
- [8] Vilarrasa, V., *et al.*, Thermal and Capillary Effects on the Caprock Mechanical Stability at In Salah, Algeria. *Greenhouse Gases Science & Technology*, 5(2015), 4, pp. 449-461
- [9] Vilarrasa, V., *et al.*, Liquid CO<sub>2</sub> Injection for Geological Storage in Deep Saline Aquifers. *International Journal of Greenhouse Gas Control*, 14(2013), 14, pp. 84-96
- [10] Mathias, S. A., *et al.*, Analytical Solution for Joule–Thomson Cooling during CO<sub>2</sub>Geo-Sequestration in Depleted Oil and Gas Reservoirs. *International Journal of Greenhouse Gas Control*, 4(2010), 5, pp.806-810
- [11] Gao, F., *et al.*, Exact Traveling-Wave Solutions for Linear and Nonlinear Heat-Transfer Equations. *Thermal Science*, 21(2017), pp. 321-321
- [12] Gor, G., *et al.*, Effects of Thermal Stresses on Caprock Integrity during CO<sub>2</sub>Storage. *International Journal of Greenhouse Gas Control*, 12(2013), 1, pp. 300-309
- [13] Wang, J. G., *et al.*, Numerical Modeling for the Combined Effects of Two-Phase Flow, Deformation, Gas Diffusion and CO<sub>2</sub>, Sorption on Caprock Sealing Efficiency. *Journal of Geochemical Exploration*, 144(2014), pp. 154-167
- [14] Wang, J. G., *et al.*, Effect of CO<sub>2</sub>Sorption-Induced Anisotropic Swelling on Caprock Sealing Efficiency. *Journal of Cleaner Production*, 103(2015), pp. 685-695
- [15] Heidaryan, E., *et al.*, Viscosity of Pure Carbon Dioxide at Supercritical Region: Measurement and Correlation Approach. *Journal of Supercritical Fluids*, 56(2011), 2, pp. 144-151
- [16] Ziabakhsh-Ganji, Z., *et al.*, Sensitivity of Joule–Thomson Cooling to Impure CO<sub>2</sub> Injection in Depleted Gas Reservoirs. *Applied Energy*, 113(2014), 6, pp. 434-451
- [17] Teng, T., *et al.*, Complex Thermal Coal-Gas Interactions in Heat Injection Enhanced CBM Recovery. *Journal of Natural Gas Science & Engineering*, 34(2016), pp. 1174-1190
- [18] Wang, H., *et al.*, A Two-phase Flowback Model for Multiscale Diffusion and Flow in Fractured Shale Gas Reservoirs. *Geofluids*, Article ID 5910437(2018), pp.1-15

Paper submitted: May 11, 2018

Paper revised: September 21, 2018

Paper accepted: November 11, 2018